analytical chemistry

pubs.acs.org/ac Article

Bovine Serum Albumin-Cross-Linked Polyaniline Nanowires for Ultralow Fouling and Highly Sensitive Electrochemical Protein Quantification in Human Serum Samples

Yang Li, Rui Han, Min Chen, Leyao Zhang, Guixiang Wang,* and Xiliang Luo*

Cite This: *Anal. Chem.* 2021, 93, 4326−4333 Read Online

ACCESS | Metrics & More | Article Recommendations | Supporting Information

ABSTRACT: Biofouling represents a serious challenge for the assaying of disease markers with various biosensors in complex biological samples due to the accompanied nonspecific protein adsorption. Herein, a highly sensitive and antifouling biosensing interface was constructed based on a cost-effective inert protein bovine serum albumin (BSA) cross-linked with polyaniline nanowires (PANI-NWs). Compared with the physically adsorbed BSA that was commonly used to block nonspecific adsorption or binding of proteins, the cross-linked BSA exhibited a significantly enhanced antifouling capability. The BSA/PANI-NW-modified electrode interface possessed excellent antifouling capability and electrochemical activity owing to the presence of the cross-linked BSA and the conducting polymer polyaniline. With further immobilization of the peptide aptamer for immunoglobulin G (IgG) recognition onto the BSA/PANI-NW interface, an electrochemical biosensor with excellent selectivity and sensitivity was prepared. The IgG biosensor possessed a linear range from 1.0 ng mL^{-1} to 10 μg mL^{-1} and a low detection limit of 0.27 ng mL^{-1}, and it was capable of assaying IgG in complex human serum samples with acceptable accuracy when compared with the assay results obtained using commercial enzyme-linked immunosorbent assay kits. It is expected that the unique BSA-cross-linked conducting polymers can be used for the construction of various electrochemical sensors and biosensors that can be applied in complex biological media.

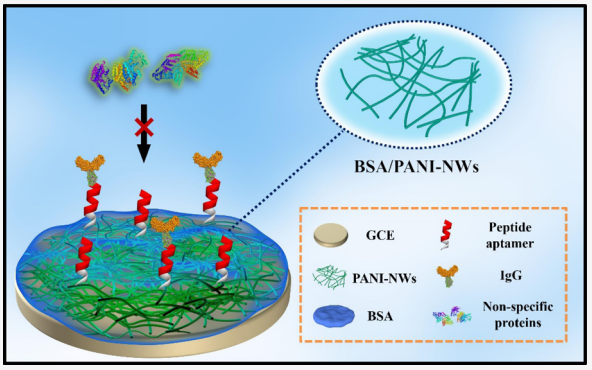

KEYWORDS: *Antifouling, Electrochemical biosensor, Bovine serum albumin, Polyaniline nanowires, IgG*

Biological fouling is a ubiquitous and undesirable effect that refers to the nonspecific adsorption of biological substances or macromolecules (such as proteins and microbes) on specific surfaces. It is not limited to industrial production but is involved in several fields of life science and clinical medicine such as implantable devices and real-time monitoring biosensors.[1,2] In particular, it is of vital practical significance to prevent biofouling in complex environments in vivo using biosensing devices for the monitoring and diagnosis of diseases. The modification of specific surfaces or interfaces with different antifouling biomaterials has been proved to be an effective method to resist the disturbances caused by biological contaminants.[3,4]

Thus far, various antifouling materials have been explored as well extensively investigated in the biomedical context.[3] Due to their characteristics of strong hydrophilicity and electroneutrality, certain classic antifouling materials such as poly(ethylene glycol) (PEG)[5−7] and zwitterionic polymers[8−10] have been widely used to reduce nonspecific protein adsorption. However, these antifouling materials either possess limited stability in biological media (PEGs tend to be degraded by certain enzymes in serum) or require complicated synthesis conditions, which greatly constrains their practical applications.[11,12]

Recently, novel antifouling biomaterials have been synthesized and utilized for the construction of effective antifouling biosensors.[13] For example, amphiphilic peptides, on account of their superior biocompatibility and functional diversity, have been widely used in biological medicine and technology, including designing peptide-based antifouling biosensors for biomarker detection in complex biological media, and many efforts have been devoted by researchers worldwide in this regard. Our group has also designed a series of multifunctional peptide sequences with strong hydrophilicity, electrical neutrality, and other specific functions to construct electrochemical biosensors capable of assaying different biomarkers in

Received: January 8, 2021
Accepted: February 16, 2021
Published: February 26, 2021

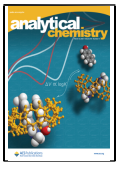

https://dx.doi.org/10.1021/acs.analchem.1c00089
Anal. Chem. 2021, 93, 4326−4333

Scheme 1. Schematic Illustration of the Fabrication Process of the Electrochemical IgG Biosensor Based on a BSA/PANI-NW Antifouling Interface

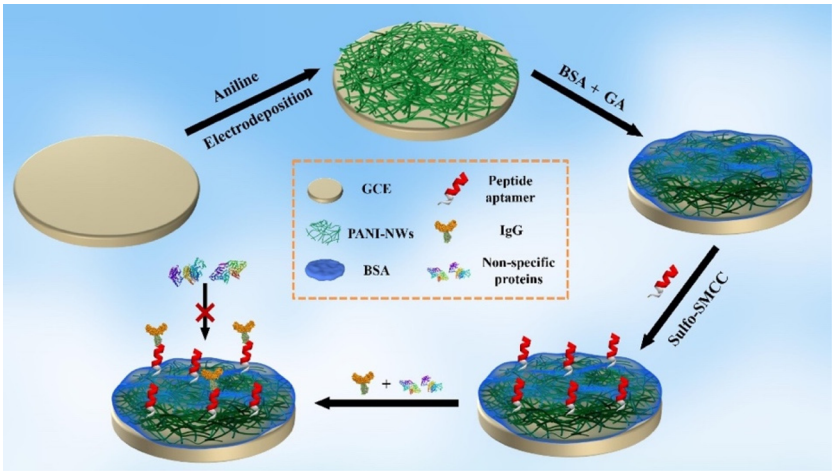

biological fluids (e.g., human serum) by taking advantage of their excellent antifouling capabilities.[14−16] Of note, in spite of their well-established synthesis pathway and preparation methods, the common techniques for peptide synthesis such as solid-phase synthesis usually involve time-consuming and labor-intensive preparation routes, like protection of reactive groups and purification steps, which also result in the high cost of application.[17,18]

Serum albumins (SAs) are one of the most widely abundant protein components in the body, both in animals and human beings.[19,20] Such multifunctional proteins are often found in the blood and have structural homology and similar functionality to those in different bodies, such as human serum albumin (HSA) and bovine serum albumin (BSA), which can maintain hematological osmolality and be used to store or transport a series of bioactive molecules and drugs.[21−24] In addition, due to the conservation of both amino acid sequences and a three-dimensional structure,[25] SAs are well known as a stable and widely applicable antifouling material to resist nonspecific protein adsorption and often are used as passivators or blockers for biosensing devices and platforms, like electrochemical biosensors.[26,27] Among them, BSA is the most widely used SA to passivate or block active sites on the electrochemical sensing interfaces,[28,29] considering its unique features of abundance, low cost, low immunogenicity, and superior biocompatibility. In most cases, BSA physically adsorbed onto the sensing interfaces to block the active sites via incubation of biosensors or devices in a BSA solution with a high concentration, and the adsorbed BSA did prevent further nonspecific protein adsorption to some degree. However, the physically adsorbed BSA cannot ensure full blocking of the active surfaces, which is not suitable for highly sensitive sensing devices, and the adsorbed BSA may also detach from the surfaces gradually, leading to unreliable sensing signals. In addition, for electrochemical sensing platforms, the physically adsorbed BSA may hinder electron transfer in the interfaces, resulting in a poor electrochemical signal and low sensitivity.

Herein, we constructed an effective antifouling electrochemical biosensor capable of detecting proteins in serum samples based on BSA. To enhance the antifouling capability of BSA and increase its stability, BSA was cross-linked and chemically attached to the modified electrode surface. In order to alleviate the blocking effect of BSA on the conductivity or electron transfer of the sensing interface, the conducting polymer polyaniline nanowires (PANI-NWs) were electrodeposited on the electrode surface, and BSA was cross-linked within the PANI-NW network to form an antifouling and conducting interface with a three-dimensional pore structure (BSA/PANI-NWs), as shown in Scheme 1. As BSA is a commercially available and considerably cheap protein, the construction of this antifouling interface is generally cost-effective. With further immobilization of the peptide aptamer (CPPPPHWRGWVA) to identify immunoglobulin G (IgG), as an important biomarker of cancer and COVID-19,[30−32] a highly sensitive and antifouling electrochemical biosensor was fabricated, and reliable IgG quantification was achieved in complex biological media like human serum and human blood samples.

EXPERIMENTAL SECTION

Reagents. An aniline monomer was purchased from Aladdin Biochemical Technology Co., Ltd. (Shanghai, China). Glutaraldehyde (GA) was obtained from Macklin Biochemical Co., Ltd. (Shanghai, China). BSA was provided by Adamas-Beta Reagent (Shanghai, China). The recognizing peptide (sequence of CPPPPHWRGWVA) was synthesized (purity >95%) and provided by Bankpeptide Biological Technology Co., Ltd. (Hefei, China), which was examined by high-performance liquid chromatography, and the mass spectra are shown in Figure S1 of the Supporting Information. 4-(*N*-Maleimidomethyl) cyclohexane-1-carboxylic acid 3-sulfo-*N*-hydroxy-succinimide ester sodium salt (sulfo-SMCC) was used as a coupling agent (Sigma-Aldrich, USA). Human immunoglobulin G (IgG) (>97%), human immunoglobulin M (IgM), carbohydrate antigen 15−3 (CA15−3), alpha fetoprotein (AFP), carcinoembryonic antigen (CEA), lysozyme (Lys), hemoglobin (Hb), and HSA were provided by Solarbio Science & Technology Co., Ltd. (Beijing, China). Roswell Park Memorial Institute 1640 medium (RPMI-1640 medium) was purchased for cell culture from Sigma Co., Ltd. (Aldrich, St. Louis, MO, USA). Dulbecco's phosphate buffered saline (DPBS) was purchased from Coolaber Science & Technology (Beijing, China). Fluorescein diacetate (FDA) and fluorescein isothiocyanate-labeled BSA (FITC-BSA) were used for the antifouling experiments and purchased from Sangon Co., Ltd.

https://dx.doi.org/10.1021/acs.analchem.1c00089
Anal. Chem. 2021, 93, 4326−4333

(Shanghai, China). Fetal bovine serum (FBS) was purchased from Evergreen Co., Ltd. (Hangzhou, China). Serum samples from healthy persons and patients were obtained from Eighth People's Hospital of Qingdao (Qingdao, China) as well as following the compliance with hospital guidelines and related regulations. IgG from serum samples of patients was assessed using commercial enzyme-linked immunosorbent assay (ELISA) kits (Meimian, Jiangsu, China) for comparison. Other chemicals were analytically pure reagents, and all solutions used in the experiment were prepared with pure water with a resistivity of >18 MΩ cm, which was produced by the water purification system (Milli-Q water system, Bedford, MA, USA).

Apparatus. The electrochemical characterizations were carried out using a three-electrode system associated with a CHI 660E electrochemical workstation (Shanghai CH Instrument Co., China) at an ambient temperature. For the three-electrode system, the working electrode was a glassy carbon electrode (GCE), the reference electrode was a saturated calomel electrode, and the auxiliary electrode was a platinum wire. The chronopotentiometry (CP) technique was used for the electrodeposition of PANI-NWs. The current signals of the different modified electrodes were recorded in a phosphate buffered saline (PBS, 0.2 M, pH 7.4) by differential pulse voltammetry (DPV) and cyclic voltammetry(CV) with the CHI 660E electrochemical workstation. The cycling potential of CV was between −0.6 and 0.6 V with a scan rate of 0.10 V s^{-1}, and the potential range of DPV was from −0.6 to 0.6 V at a pulse period of 0.2 s, an amplitude of 50 mV, and a potential increment of 4.0 mV.

Scanning electron microscopy (SEM) and mapping characterization were performed using the Hitachi Regulus 8100 scanning electron microscope (Hitachi Co., Ltd., Japan). A TCS-SP5 confocal microscope (Leica, Germany) was used for protein adsorption characterization by fluorescence imaging. Circular dichroism(CD) spectra for detecting the secondary structure of the peptide aptamer were recorded using a JASCO J-810 spectropolarimeter (Jasco Inc., Japan). The IgG assay for the serum samples of patients was performed using the ELISA kit, and the corresponding absorbance values were recorded with an EPOCH2 microplate reader (BioTek Instruments, Winooski, VT, USA) with built-in Gen5 software (Version 3.08, BioTek Instruments) for collecting and analyzing the data. X-ray photoelectron spectroscopy (XPS) spectra were collected using a Thermo ESCALAB 250Xi spectrometer (Thermo Fisher Scientific, VT, USA), with a corresponding monochromatic Al Kα X-ray source (hν = 15 kV) and a normalized spectra value of C 1 s peak of 284.6 eV. Furthermore, an MST-80 thermostatic incubator (Taitan, China) was employed to ensure a suitable and accurate incubation temperature.

Preparation of a BSA/PANI-NW Antifouling Interface. GCE was first polished using 0.3 and 0.05 μm Al_2O_3 slurry and cleaned with an ultrasonic bath in Millipore water, ethanol, and again Millipore water for 2 min, respectively. Afterward, for the preparation of the BSA/PANI-NW antifouling interface, PANI-NWs were first electrodeposited onto the pretreated GCE using the galvanostatic technique of CP and then immersed in a 0.5 M aniline solution containing 1.0 M $HClO_4$. The different current densities were controlled to 0.6, 0.3, and 0.15 mA cm^{-2}, and the corresponding time periods of electrodeposition were selected as 0.5, 0.5, and 0.5 h, respectively.[33] Then, the prepared PANI-NW-modified electrode (PANI-NW/GCE) was washed with Millipore water and soaked in 12 mg mL^{-1} of BSA and 5% GA solution (volume ratio 1:1) at 37 °C for 16 h, where GA was used as a cross-linker that enables amino-group cross-linking between BSA and PANI-NWs. The final antifouling interface of the BSA/PANI-NW (GA cross-linking)-modified electrode (BSA/PANI-NW/GCE) was thus prepared. In addition, PANI-NW/GCE was soaked in 6.0 mg mL^{-1} of BSA solution at 37 °C for 16 h and the other conditions were same as BSA/PANI-NW (GA cross-linking); thus, the BSA/PANI-NW (physical adsorption)-modified electrode was prepared.

Fabrication of the IgG Biosensor. The prepared BSA/PANI-NW/GCE antifouling interface was soaked in 2.0 mM aqueous solution of sulfo-SMCC as a cross-linker for 1 h at room temperature. Subsequently, the antifouling interface was incubated in 0.2 mg mL^{-1} of an IgG peptide aptamer solution for 3 h. The connection between the peptide aptamer and the antifouling interface was achieved by covalent bonding between Cys-terminal thiols of the peptide aptamer and the amino groups of BSA.[34] After thorough washing with Millipore water, the IgG biosensor (Pep/BSA/PANI-NW/GCE) was obtained successfully.

Characterization of the Antifouling Performance. To evaluate the antifouling ability, the changed DPV signals of the antifouling interface and the IgG biosensor were recorded, before and after incubation in different diluted concentrations (v/v) of human serum and human blood samples, with an immersion time of half an hour followed by thorough washing with Millipore water, and then the signal values were recorded in PBS. Human serum and blood samples were diluted with PBS (10.0 mM, pH 7.4) to different concentrations.

In addition, the adsorption of FITC-BSA was also measured for assessing the protein adsorption degree on the surfaces of the modified electrodes and IgG biosensor, and PANI-NW-modified surfaces were used as a control. A TCS-SP5 confocal laser microscope with an excitation light wavelength of 488 nm and an FITC-BSA emission wavelength of 525 nm was used for fluorescence imaging. All modified interfaces were incubated before fluorescence imaging in 1.0 mg mL^{-1} of FITC-BSA solution at 37 °C for 24 h.

Cell Culture and Cell Adhesion Test. For cell adhesion testing, healthy human embryonic kidney 293 cell lines (HEK 293 cell lines) were cultured in the RPMI-1640 medium, supplemented with 10% (v/v) FBS and 1% dual antibiotics of penicillin and streptomycin, where the HEK 293 cells were cultured in an incubator by maintaining a certain degree of humidity and 5.0% CO_2 at 37 °C. After culturing for 24 h, the RPMI-1640 medium was changed with a fresh one and the cells were further cultured for 24 h, and then the HEK 293 cells were detached using a trypsinization solution containing 0.25% trypsin and 0.02% EDTA. HEK 293 cells were separated from the RPMI-1640 medium via low-speed centrifugation at 800 rpm, and the statistical cell number was measured using a hemocytometer.

The prepared HEK 293 cell lines were cocultured together with the surfaces of the antifouling interface, IgG biosensor, and PANI-NW-modified electrode for 24 h under the same conditions. After rinsing with DPBS, the level of adhesion of the active HEK 293 cell lines stained with FDA (50.0 μg mL^{-1}) on the different surfaces was assessed, where the fluorescence images were captured using the TCS-SP5 confocal laser microscope with an excitation wavelength of

https://dx.doi.org/10.1021/acs.analchem.1c00089
Anal. Chem. 2021, 93, 4326−4333

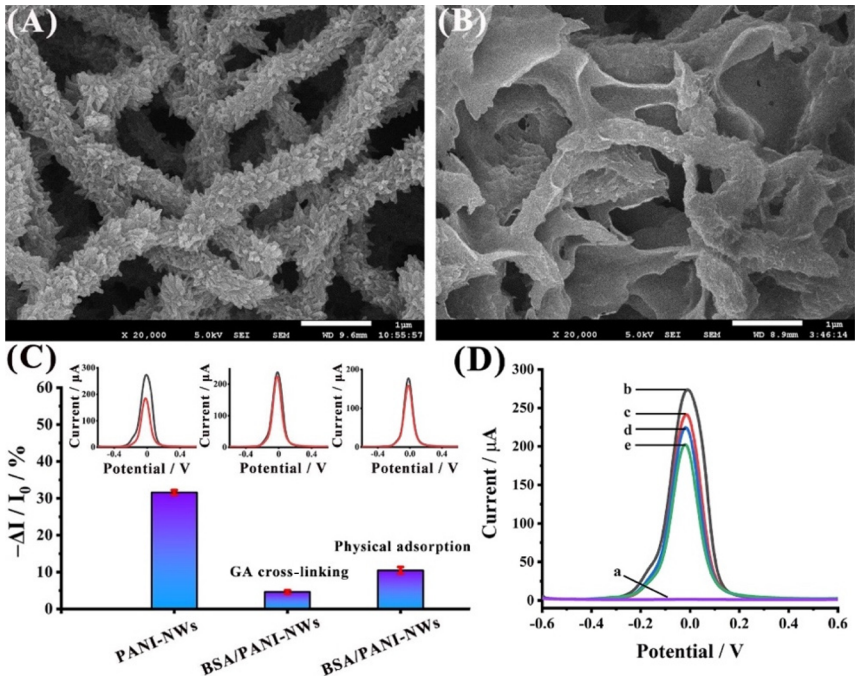

Figure 1. SEM images of electrodeposited (A) PANI-NWs and (B) BSA/PANI-NW-modified antifouling interface.(C) Antifouling performance of PANI-NW/GCE, BSA/PANI-NW/GCE (GA cross-linking), and BSA/PANI-NW/GCE (physical adsorption) in 100% healthy human serum samples. The inset shows relevant DPV curves before (black) and after (red) incubation in 100% human serum samples and the DPV curves were measured in PBS (0.2 M, pH 7.4). (D) DPV responses of different modified electrodes (a) GCE, (b) PANI-NW/GCE, (c) BSA/PANI-NW/GCE, (d) Pep/BSA/PANI-NW/GCE, and (e) IgG/Pep/BSA/PANI-NW/GCE in PBS (0.2 M, pH 7.4).

488 nm and the emission wavelength of FDA (530 nm) was used for fluorescence imaging.

Sensing with the IgG Biosensor. In order to accomplish quantitative analysis of IgG, a series of concentrations of target IgG were diluted with PBS solution (10.0 mM, pH 7.4) to obtain the IgG standard samples. The prepared biosensor was incubated in IgG solutions of different concentrations for 90 min at 37 °C. DPV was used to monitor the electrochemical signal changes in PBS (0.2 M, pH 7.4) for the biosensor before and after incubation in the IgG solution in the potential range of −0.6 to 0.6 V.

To evaluate the practical application potential of this antifouling IgG biosensor in real biological samples, a series of concentrations of IgG were diluted with 100% (v/v) FBS solution. Subsequently, electrochemical assays were performed under the same conditions for the detection of IgG standard samples; meanwhile, the DPV signal changes before and after incubation were monitored and recorded.

Analysis of Real Serum Samples and Contrasting Approaches. Fresh blood samples from five patients were preprocessed by centrifugation at 10,000 rpm for 5 min, and the supernatants were collected to obtain patient serum samples. Subsequently, the quantitative analysis of IgG in the patient serum samples was carried out using the designed IgG biosensor, and the commercial ELISA kits were used as a reference.

RESULTS AND DISCUSSION

Synthesis and Characterization of the BSA/PANI-NW Antifouling Interface. To enhance the electrochemical signal, PANI-NWs as a conductive substrate were first electrodeposited. Subsequently, BSA was successfully cross-linked with PANI-NWs by GA, forming an antifouling interface with a three-dimensional pore structure and good conductive performance. To achieve better antifouling properties, the concentration and incubation time of BSA were optimized, as shown in Figure S2. According to the signal change rate ($-\Delta I/I_0$, $\Delta I = I - I_0$, I_0 and I represent the DPV signals before and after incubation with different concentrations of serum samples) of the modified electrode after soaking in a 100% serum sample for 30 min, 10 mg mL^{-1} was selected as the final concentration of BSA, and the incubation time was 16 h. It is clear that the lower BSA concentration was associated with a poorer antifouling performance. We speculated that a very low BSA concentration or a very short reaction time will lead to the formation of a much thinner BSA film, and the presence of some residual nonreacted GA on the electrode surface may react with other proteins, resulting in a poor antifouling capability.[35]

The morphological change of PANI-NWs combined with BSA was characterized by SEM. As shown in Figure 1A and Figure S3, the prepared PANI-NWs possessed a three-dimensional porous network structure with a large surface area, which is beneficial for a higher electron transfer rate.[33] After the cross-linking of BSA, the obtained BSA/PANI-NW surface showed a significant morphology change, and clear BSA attachment between nanowires was observed (Figure 1B). The BSA/PANI-NWs retained a porous network structure and exhibited excellent antifouling ability (Figure 1C). However, for normal physical adsorption of BSA in the absence of GA, BSA will gather excessively on the surface of PANI-NWs, resulting in a poor antifouling performance, as shown in Figure 1C and Figure S4.

XPS was also used to verify the successful cross-linking of BSA and PANI-NWs. As shown in Figure S5A, for the PANI-NW surface, C 1s, O 1s, and N1 s signal peaks were observed.

https://dx.doi.org/10.1021/acs.analchem.1c00089
Anal. Chem. 2021, 93, 4326−4333

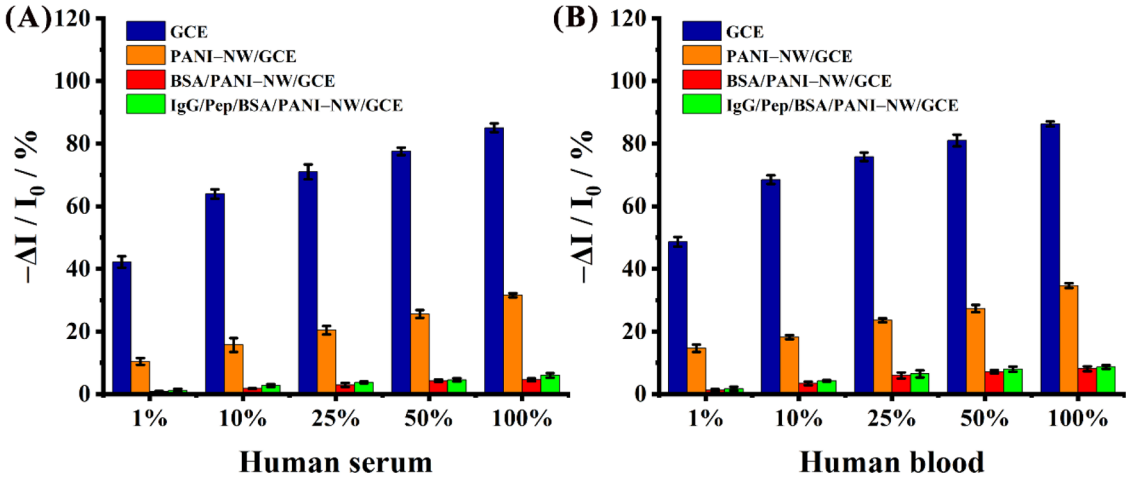

Figure 2. Current signal change rates of GCE, PANI-NW/GCE, BSA/PANI-NW/GCE (antifouling interface), and IgG/Pep/BSA/PANI-NW/GCE (IgG biosensor) in a series of healthy human serum (A) and healthy human blood (B) samples. The IgG biosensor was first saturated with 1.0 mg mL^{-1} of IgG before incubation in healthy human serum and healthy human blood samples. Error bars represent the standard deviations of three repeated determinations.

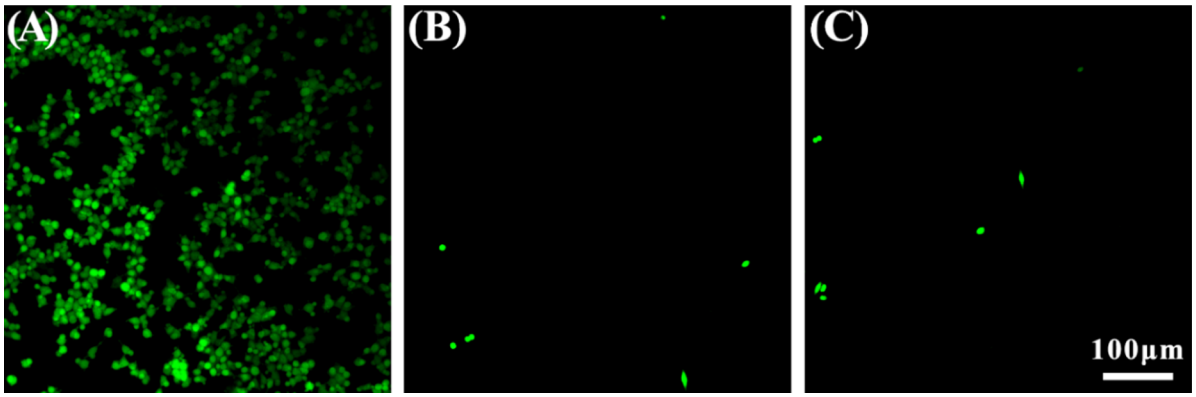

Figure 3. Fluorescence images for anti-cell attachment performance of (A) PANI-NWs, (B) BSA/PANI-NW-modified surfaces, and (C) biosensors. All the modified surfaces were co-incubated with HEK 293 cells for 24 h at 37 °C. All the images are of the same scale bar of 100 μm.

After the cross-linking of BSA, the appearance of the S 2p (164 eV) signal peak and a significant increase of the signal peak of N 1s (400 eV) indicated that BSA was cross-linked to the PANI-NW surface (Figure S5B). Meanwhile, the presence of an S element in the mapping characterization also proved the even cross-linking of BSA in an intuitive and explicit way (Figure S6).

Construction of the Electrochemical Biosensor. The biosensor fabrication process is shown in Scheme 1. PANI-NWs were electrodeposited on the GCE using the three-step deposition method, and subsequently, BSA was cross-linked to PANI-NW/GCE, forming BSA/PANI-NW/GCE with a three-dimensional antifouling interface possessing a porous structure and excellent conductivity. Then, the IgG peptide aptamer was immobilized to BSA/PANI-NW/GCE by a reaction between Cys-terminal thiols and amino groups from the antifouling interface in the presence of sulfo-SMCC, and the antifouling electrochemical IgG biosensor was thus fabricated.

The successful construction of the IgG biosensor was characterized by measuring the DPV signals of each step of the fabrication process, as shown in Figure 1D. The current signal of the electrode was significantly enhanced by the deposition of PANI-NWs compared with the bare GCE, owing to the good conductivity and large surface area of the PANI-NWs. Furthermore, the cross-linking of BSA resulted in a decrease of the DPV signal, owing to the blocking effect of BSA. Subsequently, the current signal decreased after the immobilization of the IgG peptide aptamer as the immobilized peptide aptamer further blocked the electron transfer on the electrode surface. Finally, along with the capture of the target IgG, a further decrease of the current signal was observed due to the steric hindrance effect of the IgG protein, which can be used as the signal for the sensing of IgG. As expected, the peak currents of the modified electrodes were linearly related to the scanning rate, and this result demonstrated that the redox process of the modified electrode was a surface-restricted process with rapid electron transfer kinetics (Figure S7).

Characterization of the Antifouling Performance. The antifouling properties of the PANI-NWs, BSA/PANI-NW-modified electrodes, and the biosensors were investigated using a series of concentrations of human serum and human blood samples (v/v), and the relevant DPV curves are shown in Figure S8. The current signal change rates of the four electrode surfaces are shown in Figure 2, where the signal change rates of the BSA/PANI-NW-modified electrodes and biosensors in an undiluted human serum sample (100% serum) were only 4.7 and 6.2%, respectively, while those of the bare GCE and the PANI-NW-modified electrode decreased by 83.5 and 31.3%,

https://dx.doi.org/10.1021/acs.analchem.1c00089
Anal. Chem. 2021, 93, 4326−4333

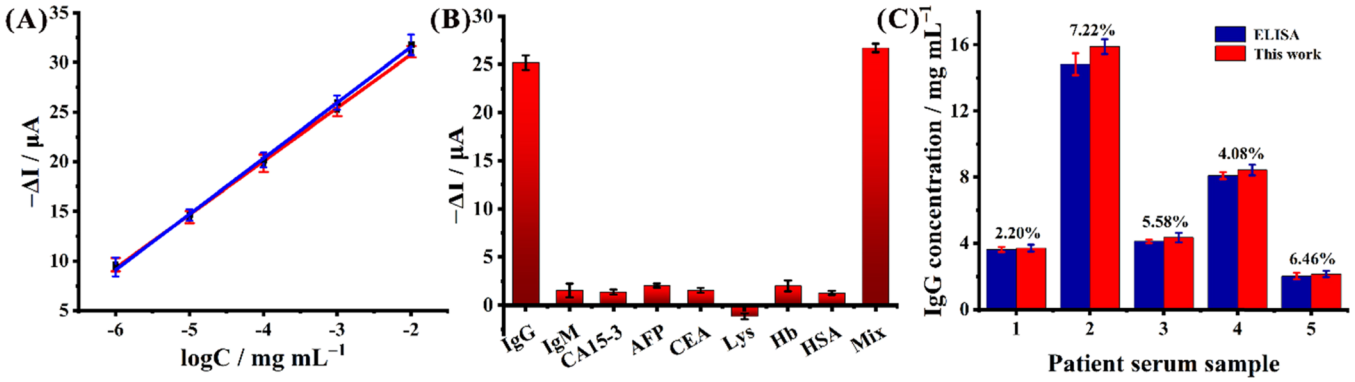

Figure 4. (A) Calibration curve of the biosensor against IgG with different concentrations diluted in 10.0 mM PBS (red) and in the presence of 100% FBS (blue). (B) Responses of the biosensor to IgG (1 μg mL^{-1}), IgM (1 mg mL^{-1}), CA15−3 (1 mg mL^{-1}), AFP (1 mg mL^{-1}), CEA (1 mg mL^{-1}), Lys (1 mg mL^{-1}), Hb (1 mg mL^{-1}), HSA (1 mg mL^{-1}), and a mixture of the abovementioned proteins. All the solutions were diluted with PBS (0.2 M, pH 7.4). (C) Assay results of clinical serum samples using ELISA and the developed method of this work. The percentage of variance between the two approaches for each clinical sample was shown above the respective data. Error bars represent the standard deviations of three repeated determinations.

respectively. The excellent antifouling performance of the BSA/PANI-NW-modified electrodes was ascribed to the presence of cross-linked BSA, which prevented soluble albumin molecules (approximately 60% of serum) from adsorbing to the electrode surface. In addition, the signal change rates of BSA/PANI-NW/GCE and the biosensor in an undiluted human blood sample (100% blood) were 7.8 and 8.4%, respectively. For both BSA/PANI-NW/GCE and the biosensor, the fouling effects were slightly higher in the human blood sample compared with the human serum sample as fibrinogen and coagulation factors are present in the human blood, which are specific components that not exist in the human serum, as well the difference in the antifouling effect between serum and blood may be induced by fibrinogen in the blood.[36]

Additional investigations of protein adsorption and cell adhesion were performed to further validate the antifouling abilities of different surfaces. First, the cell adhesion performances of PANI-NWs, BSA/PANI-NW-modified surfaces, and biosensors were investigated. As shown in Figure 3, a large amount of HEK 293 cells was found on the PANI-NW-modified surface, indicating poor antifouling properties. By contrast, very few HEK 293 cells adhered to the BSA/PANI-NW-modified surface (Figure 3B) and the IgG biosensor surface (Figure 3C), suggesting that the BSA/PANI-NW-modified interface played a crucial role in the prevention of cell adhesion. Similarly, the FITC-BSA adsorption tests also showed that few FITC-BSA adsorbed onto BSA/PANI-NW/GCE (Figure S9B) and the biosensor surface (Figure S9C), compared with the PANI-NW-modified surface (Figure S9A), suggesting excellent antifouling properties.

Investigation of the long-term antifouling ability is essential for an antifouling interface. Thus, the long-term antifouling performance of different modified electrodes in 100% human serum samples was investigated as shown in Figure S10. The results showed that the BSA/PANI-NW-modified electrodes and the biosensor have a low signal suppression rate of less than 20% within 10 days, suggesting that the prepared BSA/PANI-NW-modified electrodes and antifouling biosensors still maintained better antifouling effects than those electrodes without BSA with long exposure in complex biological media.

Sensing Performance of the IgG Biosensor. For the best sensing performance, the incubation time of the target was optimized, and 90 min was finally determined as the best incubation time (Figure S11A). Meanwhile, the IgG peptide aptamer concentration was optimized for sensing (Figure S11B) and antifouling (Figure S11C) aspects, respectively, and 0.2 mg mL^{-1} was selected as the optimal concentration of the IgG peptide aptamer.

The signal response of the sensor to IgG from 1.0 ng mL^{-1} to 10 μg mL^{-1} was measured for an optimal sensing performance (Figure S12A,B). The linear regression equation was $\Delta I = -5.38 \log(C) - 41.57$, with a correlation coefficient of 0.9989. The limit of detection (LOD) was 0.27 ng mL^{-1} (S/N = 3), which is much lower than that of previous reports (Table S1).[34,37−41] The lower LOD may be ascribed to the advantage of BSA/PANI-NWs with excellent antifouling capability and good stability, which provided a low noise signal for high specific binding of IgG. In addition, we hypothesized that the rigid conformation of the IgG peptide aptamer allows for closer packing and higher loading, where the polyproline helix conformation was determined by CD spectroscopy with a negative band at about 200 nm and a weaker positive band at around 225 nm (Figure S13).[42]

To examine the target binding ability of the biosensor in a complex medium, different concentrations of IgG solutions were formulated with 100% FBS. As can be seen in Figure 4A, the biosensor still presented good target binding ability for IgG in the complex environment, with a similar response as that in 10.0 mM pure PBS (DPV responses and calibration curves are shown in Figure S12C,D). Meanwhile, the result also reflected the excellent antifouling ability of the IgG biosensor, providing further support for practical clinical applications.

Specificity and Reproducibility of the IgG Biosensor. The selectivity of the biosensor was evaluated by detecting target IgG and a series of interfering proteins such as IgM, CA15−3, AFP, CEA, Lys, Hb, and HSA, as shown in Figure 4B. The results showed that the signal responses of the sensor to the interfering proteins were much lower than that to the specific target, and at the same time, the target IgG was detected accurately in mixture samples even though the concentrations of the interfering proteins were 1000 times the target concentration, reflecting that the biosensor possessed superior selectivity.

An electrochemical stability analysis was also performed by continuous measurement of CV at a scan rate of 0.10 V s^{-1} in

https://dx.doi.org/10.1021/acs.analchem.1c00089
Anal. Chem. 2021, 93, 4326−4333

PBS (0.2 M, pH 7.4), and the result showed that the peak current remained almost unchanged for 50 cycles (Figure S14). In addition, the prepared biosensors were immersed in PBS (0.2 M, pH 7.4) for a stability test (Figure S15A,C), and the DPV signals of the biosensors were measured every half an hour. For over seven measurements, an almost unchanged signal was observed. The long-term stability of BSA/PANI-NW/GCE and the biosensor was also investigated, and only slight changes in the signals were observed within 10 days in PBS (Figure S16). The results indicated good stability of BSA/PANI-NW/GCE and the biosensor. Additionally, the reproducibility between different biosensors prepared independently was also investigated (Figure S15B,D), and the interelectrode signal relative standard deviation was 0.69% (n = 7), indicating excellent stability and reproducibility.

Clinical Serum Sample Analysis. To investigate the practical applicability of the antifouling biosensor, IgG concentrations in serum samples from patients (diluted with 0.2 M PBS) were measured and compared with those determined by the ELISA kits, as shown in Figure 4C. The results showed that the IgG concentrations detected by the biosensors well matched with those measured by ELISA, with the difference within 8%. The results revealed that the constructed antifouling biosensor has promising potential for practical applications.

CONCLUSIONS

In conclusion, an effective antifouling electrochemical biosensing interface composed of BSA-cross-linked PANI-NWs with a three-dimensional network structure was developed for the detection of IgG in human serum samples. The cross-linked BSA showed a significantly enhanced antifouling ability, and its combination with the conducting polymer PANI supported the effective electrochemical quantification of IgG in human serum samples without suffering from biofouling. The designed electrochemical IgG biosensor showed remarkable stability and selectivity, and it shows promising potential for target IgG monitoring in complex biological media with a satisfying accuracy comparable with the well-established ELISA method. The strategy of constructing antifouling electrochemical sensing interfaces with BSA-cross-linked conducting polymers can be extended to the development of various biosensors for assaying of different targets in biological media.

ASSOCIATED CONTENT

Supporting Information

The Supporting Information is available free of charge at https://pubs.acs.org/doi/10.1021/acs.analchem.1c00089.

Chromatogram and MS spectrum of the peptide aptamer, optimization of the experiment conditions, SEM images, XPS characterization, mapping characterization, CV and DPV curves, fluorescence microscopy images, optimization of incubation time of the target and the concentration of the peptide aptamer, CD spectra, stability and reproducibility of the biosensor, and comparison with other reports (PDF)

AUTHOR INFORMATION

Corresponding Authors

Guixiang Wang − *Key Laboratory of Optic-electric Sensing and Analytical Chemistry for Life Science, MOE, Shandong Key Laboratory of Biochemical Analysis, College of Chemistry and Molecular Engineering, Qingdao University of Science and Technology, Qingdao 266042, China; College of Chemistry and Chemical Engineering, Taishan University, Taian 271021, China*; Email: wangguixiang@tsu.edu.cn

Xiliang Luo − *Key Laboratory of Optic-electric Sensing and Analytical Chemistry for Life Science, MOE, Shandong Key Laboratory of Biochemical Analysis, College of Chemistry and Molecular Engineering, Qingdao University of Science and Technology, Qingdao 266042, China*; orcid.org/0000-0001-6075-7089; Phone: +86 5328402299; Email: xiliangluo@qust.edu.cn; Fax: +8653284022681

Authors

Yang Li − *Key Laboratory of Optic-electric Sensing and Analytical Chemistry for Life Science, MOE, Shandong Key Laboratory of Biochemical Analysis, College of Chemistry and Molecular Engineering, Qingdao University of Science and Technology, Qingdao 266042, China*

Rui Han − *Key Laboratory of Optic-electric Sensing and Analytical Chemistry for Life Science, MOE, Shandong Key Laboratory of Biochemical Analysis, College of Chemistry and Molecular Engineering, Qingdao University of Science and Technology, Qingdao 266042, China*

Min Chen − *Key Laboratory of Optic-electric Sensing and Analytical Chemistry for Life Science, MOE, Shandong Key Laboratory of Biochemical Analysis, College of Chemistry and Molecular Engineering, Qingdao University of Science and Technology, Qingdao 266042, China*

Leyao Zhang − *Key Laboratory of Optic-electric Sensing and Analytical Chemistry for Life Science, MOE, Shandong Key Laboratory of Biochemical Analysis, College of Chemistry and Molecular Engineering, Qingdao University of Science and Technology, Qingdao 266042, China*

Complete contact information is available at: https://pubs.acs.org/10.1021/acs.analchem.1c00089

Notes

The authors declare no competing financial interest.

ACKNOWLEDGMENTS

We acknowledge financial support from the National Natural Science Foundation of China (21974075 and 21675093), the Science and Technology Benefiting the People Project of Qingdao (20-3-4-53-nsh), the Taishan Scholar Program of Shandong Province of China (ts20110829), the Shandong Provincial Natural Science Foundation (ZR2019MB039), the Shandong Key Laboratory of Biochemical Analysis (SKLBA1905), and the Doctoral Found of Taishan University (Y-01-2018018).

REFERENCES

(1) Jiang, S.; Cao, Z. *Adv. Mater.* **2010**, *22*, 920−932.
(2) Wei, Q.; Becherer, T.; Angioletti-Uberti, S.; Dzubiella, J.; Wischke, C.; Neffe, A. T.; Lendlein, A.; Ballauff, M.; Haag, R. *Angew. Chem., Int. Ed.* **2014**, *53*, 8004−8031.
(3) Jiang, C.; Wang, G.; Hein, R.; Liu, N.; Luo, X.; Davis, J. J. *Chem. Rev.* **2020**, *120*, 3852−3889.
(4) Banerjee, I.; Pangule, R. C.; Kane, R. S. *Adv. Mater.* **2011**, *23*, 690−718.
(5) Emilsson, G.; Schoch, R. L.; Feuz, L.; Hook, F.; Lim, R. Y.; Dahlin, A. B. *ACS Appl. Mater. Interfaces* **2015**, *7*, 7505−7515.
(6) Akbari, A.; Yegani, R.; Pourabbas, B. *Colloids Surf., A* **2015**, *484*, 206−215.

(7) Konradi, R.; Acikgoz, C.; Textor, M. *Macromol. Rapid Commun.* **2012**, *33*, 1663−1676.
(8) He, M.; Gao, K.; Zhou, L.; Jiao, Z.; Wu, M.; Cao, J.; You, X.; Cai, Z.; Su, Y.; Jiang, Z. *Acta Biomater.* **2016**, *40*, 142−152.
(9) Xia, Y.; Adibnia, V.; Huang, R.; Murschel, F.; Faivre, J.; Xie, G.; Olszewski, M.; De Crescenzo, G.; Qi, W.; He, Z.; Su, R.; Matyjaszewski, K.; Banquy, X. *Angew. Chem., Int. Ed.* **2019**, *58*, 1308−1314.
(10) Schlenoff, J. B. *Langmuir* **2014**, *30*, 9625−9636.
(11) Knowles, B. R.; Wagner, P.; Maclaughlin, S.; Higgins, M. J.; Molino, P. J. *ACS Appl. Mater. Interfaces* **2017**, *9*, 18584−18594.
(12) Wang, G.; Han, R.; Li, Q.; Han, Y.; Luo, X. *Anal. Chem.* **2020**, *92*, 7186−7193.
(13) Lin, P.-H.; Li, B.-R. *Analyst* **2020**, *145*, 1110−1120.
(14) Han, R.; Wang, G.; Xu, Z.; Zhang, L.; Li, Q.; Han, Y.; Luo, X. *Biosens. Bioelectron.* **2020**, *164*, No. 112317.
(15) Song, Z.; Chen, M.; Ding, C.; Luo, X. *Anal. Chem.* **2020**, *92*, 5795−5802.
(16) Liu, N.; Song, J.; Lu, Y.; Davis, J. J.; Gao, F.; Luo, X. *Anal. Chem.* **2019**, *91*, 8334−8340.
(17) Jad, Y. E.; Kumar, A.; El-Faham, A.; de la Torre, B. G.; Albericio, F. *ACS Sustainable Chem. Eng.* **2019**, *7*, 3671−3683.
(18) Schwieter, K. E.; Johnston, J. N. *J. Am. Chem. Soc.* **2016**, *138*, 14160−14169.
(19) Ma, G. J.; Ferhan, A. R.; Jackman, J. A.; Cho, N.-J. *Commun. Mater.* **2020**, *1*, 45.
(20) Fang, B.; Ling, Q.; Zhao, W.; Ma, Y.; Bai, P.; Wei, Q.; Li, H.; Zhao, C. *J. Membr. Sci.* **2009**, *329*, 46−55.
(21) Yu, Z.; Yu, M.; Zhang, Z.; Hong, G.; Xiong, Q. *Nanoscale Res. Lett.* **2014**, *9*, 343.
(22) Bronze-Uhle, E. S.; Costa, B. C.; Ximenes, V. F.; Lisboa-Filho, P. N. *Nanotechnol. Sci. Appl.* **2017**, *10*, 11−21.
(23) Sripriyalakshmi, S.; Anjali, C. H.; George, P. D.; Rajith, B.; Ravindran, A. *PLoS One* **2014**, *9*, No. e86317.
(24) Ikeda, M.; Ueda-Wakagi, M.; Hayashibara, K.; Kitano, R.; Kawase, M.; Kaihatsu, K.; Kato, N.; Suhara, Y.; Osakabe, N.; Ashida, H. *Molecules* **2017**, *22*, 314.
(25) Chruszcz, M.; Mikolajczak, K.; Mank, N.; Majorek, K. A.; Porebski, P. J.; Minor, W. *Biochim. Biophys. Acta, Gen. Subj.* **2013**, *1830*, 5375−5381.
(26) Park, J. H.; Jackman, J. A.; Ferhan, A. R.; Ma, G. J.; Yoon, B. K.; Cho, N.-J. *ACS Appl. Mater. Interfaces* **2018**, *10*, 32047−32057.
(27) Sweryda-Krawiec, B.; Devaraj, H.; Jacob, G.; Hickman, J. J. *Langmuir* **2004**, *20*, 2054−2056.
(28) Chaturvedi, S. K.; Ma, J.; Zhao, H.; Schuck, P. *Nat. Protoc.* **2017**, *12*, 1777−1791.
(29) Tian, C.; Wang, L.; Luan, F.; Fu, X.; Zhuang, X.; Chen, L. *Chem. Commun.* **2019**, *55*, 12479−12482.
(30) Zhang, Y.; Carbonell, R. G.; Rojas, O. J. *Biomacromolecules* **2013**, *14*, 4161−4168.
(31) Yang, H.; Gurgel, P. V.; Carbonell, R. G. *J. Chromatogr. A* **2009**, *1216*, 910−918.
(32) Hou, H.; Wang, T.; Zhang, B.; Luo, Y.; Mao, L.; Wang, F.; Wu, S.; Sun, Z. *Clin. Transl. Immunol.* **2020**, *9*, No. e1136.
(33) Hui, N.; Sun, X.; Niu, S.; Luo, X. *ACS Appl. Mater. Interfaces* **2017**, *9*, 2914−2923.
(34) Liu, N.; Hui, N.; Davis, J. J.; Luo, X. *ACS Sens.* **2018**, *3*, 1210−1216.
(35) Sabate Del Rio, J.; Henry, O. Y. F.; Jolly, P.; Ingber, D. E. *Nat. Nanotechnol.* **2019**, *14*, 1143−1149.
(36) Zhang, Z.; Zhang, M.; Chen, S.; Horbett, T. A.; Ratner, B. D.; Jiang, S. *Biomaterials* **2008**, *29*, 4285−4291.
(37) Qi, H.; Wang, C.; Cheng, N. *Microchim. Acta* **2010**, *170*, 33−38.
(38) Dong, S.; Li, M.; Wei, W.; Liu, D.; Huang, T. *J. Solid State Electrochem.* **2017**, *21*, 793−801.
(39) Huang, Y.; Wen, Y.; Baryeh, K.; Takalkar, S.; Lund, M.; Zhang, X.; Liu, G. *Anal. Chim. Acta* **2017**, *993*, 79−86.
(40) Mars, A.; Parolo, C.; Raouafi, N.; Boujlel, K.; Merkoçi, A. *J. Mater. Chem. B* **2013**, *1*, 2951−2955.
(41) Liu, C.; Cai, Q.; Xu, B.; Zhu, W.; Zhang, L.; Zhao, J.; Chen, X. *Biosens. Bioelectron.* **2017**, *94*, 200−206.
(42) Nowinski, A. K.; Sun, F.; White, A. D.; Keefe, A. J.; Jiang, S. *J. Am. Chem. Soc.* **2012**, *134*, 6000−6005.

https://dx.doi.org/10.1021/acs.analchem.1c00089
Anal. Chem. 2021, 93, 4326−4333